Optics Letters

Generation of vector beams with arbitrary spatial variation of phase and linear polarization using plasmonic metasurfaces

Ping Yu,[1] Shuqi Chen,[1,*] Jianxiong Li,[1] Hua Cheng,[1] Zhancheng Li,[1] Wenwei Liu,[1] Boyang Xie,[1] Zhaocheng Liu,[1] and Jianguo Tian[1,2]

[1]Laboratory of Weak Light Nonlinear Photonics, Ministry of Education, School of Physics and Teda Applied Physics Institute, Nankai University, Tianjin 300071, China
[2]e-mail: jjtian@nankai.edu.cn
*Corresponding author: schen@nankai.edu.cn

Received 26 May 2015; revised 11 June 2015; accepted 12 June 2015; posted 12 June 2015 (Doc. ID 241670); published 2 July 2015

A novel method is proposed to generate vector beams with arbitrary spatial variation of phase and linear polarization at the nanoscale using compact plasmonic metasurfaces with rectangular nanoapertures. The physical mechanism underlying the simultaneous control of light polarization and phase is explained. Vector beams with different spiral phasefronts are obtained by manipulating the local orientation and geometric parameters of the metasurfaces. In addition, radially and azimuthally polarized vector beams and double-mode vector beams are achieved through completely compensating for the Berry phase, which provides additional degrees of freedom for beam manipulation.

OCIS codes: (160.3918) Metamaterials; (240.6680) Surface plasmons; (260.0260) Physical optics.

http://dx.doi.org/10.1364/OL.40.003229

Metasurfaces, due to their unique electromagnetic characteristics, have drawn significant attention from scientists. Owing to the precise control of light polarization and phase, various kinds of plasmonic metasurfaces have been proposed in the applications of anomalous refraction or reflection [1,2], holographic imaging [3], vortex beam generation [4–8], polarization conversion [9–11], etc. Recently, vector beams have attracted significant interest owing to their distinct features and interesting properties. The spatially variant polarization states of vector beams can potentially be used in various applications in optical trapping and manipulation [12–14], light focusing [15,16], nonlinear optics [17], particle acceleration [18], and so on. As a result of these peculiar properties and extensive applications, several conventional methods have been proposed to generate vector beams, such as spatial light modulation [19,20], interferometry [21], and the use of spatially variant subwavelength gratings [22]. Despite the successful generation of vector beams using these methods, several problems still remain: (1) the employed devices are bulky; (2) the generated beams are always unstable or have low efficiency; and (3) the generated beams cannot be suppressed at the nanoscale, which limits their applications.

Scientists have attempted to overcome these disadvantages by using plasmonic metasurfaces. For example, vector beams carrying orbital angular momentum can be obtained by using nanoscale single-layer metasurfaces [23–27]. The polarization distributions can be easily manipulated by spatially arranging the orientations of these metasurfaces. However, an additional phase (Berry phase) is introduced to the transmitted light in the process of polarization manipulation [28]. Because of the lack of any effective phase manipulation to compensate for the Berry phase, the generated vector beams always carry helical phase distributions. As a result, it is still a great challenge to generate the standard radially and azimuthally polarized vector beams. Another method to generate cylindrical vector vortex beams has been investigated by utilizing two separated metasurfaces [29]. This method requires the rigorous alignment of two separate metasurfaces, and the whole device is difficult to integrate. Therefore, searching for a feasible way to simultaneously control the polarization and phase of light at the nanoscale is necessary.

In this Letter, we demonstrate a novel method for generating vector beams at the nanoscale through the use of compact plasmonic metasurfaces with rectangular nanoapertures. By means of manipulating the local orientation and geometric parameters of the metasurfaces, the light polarization can be varied across the range of 360°, and the phase can be manipulated throughout the entire 360° range. Furthermore, radially polarized vector beams with different spiral phasefronts can be obtained through simultaneous control of linear polarization and phase of the transmitted light. The standard radially and azimuthally polarized vector beams, together with the double-mode vector beam, also can be generated by completely compensating for the Berry phase.

0146-9592/15/143229-04$15/0$15.00

Figures 1(a) and 1(b) schematically illustrate unit cells of the proposed metasurfaces with rectangular nanoapertures. Two layers (120 nm thick) are separated by 100 nm along the z axis; the top and bottom nanoapertures are either aligned or laterally translated by S in the y direction. The optical parameter of gold is described by a Drude model with a relative permittivity of $\varepsilon_\infty = 9.0$, a plasma frequency of $\omega_p = 1.3166 \times 10^{16}$ s^{-1}, and a damping constant of $\gamma = 1.3464 \times 10^{14}$ s^{-1} [30]. The whole structure is embedded within silicon dioxide, whose dielectric constant is 2.25. The 3D finite element method was utilized in our numerical simulations with COMSOL Multiphysics [31]. The corner effect of rectangular nanoapertures has been considered in the simulation with a curvature radius of 6 nm.

When illuminating with a normally incident circularly polarized (CP) plane wave, the phase of the transmitted light can be conveniently manipulated by changing the length L of the rectangular nanoaperture due to the local resonance of excited surface plasmon polaritons (SPPs) [32]. The range of phase shifting can be further extended by tuning the lateral translation S. An SPP standing wave can be formed because of the coupling between the two metal layers. When the lateral translation $S = P_y/2$, where P_y is the period in the y directions, the charge oscillations at the bottom nanoapertures will exhibit opposite direction compared with those of $S = 0$. Thus, the transmitted light has a phase difference close to 180° for the two cases of $S = 0$ and $S = P_y/2$, as shown in Figs. 1(c) and 1(d). Meanwhile, the field component along the major axis of a rectangular nanoaperture will be simply filtered out based on the anisotropic polarization response. The proposed dual-layer metasurface can be regarded as an effective local linear polarizer. The calculated transmissions parallel and vertical to the major axis of a nanoaperture for $S = 0$ and $S = P_y/2$ when excited by normally incident CP light are illustrated in Figs. 1(e) and 1(f), respectively. There only exists a transmitted light polarized vertical to the major axis of the nanoaperture in a broadband wavelength range for the two cases. Therefore, the phase variation spanning over the entire 360° range can be easily achieved by tuning the rectangular length L and controlling the lateral translation S to change the existing waveguide mode between dual-layer nanoapertures. Linearly polarized (LP) light with an arbitrary polarization direction can be obtained by rotating the unit cells of the plasmonic metasurfaces. Considering the fabricated process, a slight change of the parameter such as the lateral translation S, dielectric thickness between two layers, and the curvature radius of corners has a little influence on the presented polarization and phase properties.

We adopted a system of 12 units to generate the vector beams in Fig. 2. The lateral translation S for the first and second six units is 0 and 225 nm, respectively. The transmitted phase can be controlled by tuning parameters L and S, while uniform transmissions for 12 units can be obtained by adjusting parameter W. Figure 2(a) illustrates the transmitted phase and amplitude of 12 units under CP incident light at the wavelength of 850 nm. The transmission phase of the units controlled by structural parameters covers the entire 360° range with an interval of 30°; all units have a similar transmission amplitude of around 28% when the rotation angle of the units is fixed. We also extracted the ellipticity e (the minor-to-major-axis ratio) and the polarization directions of transmitted light, as shown in Fig. 2(b). The results show that the ellipticity of transmitted light is always around the minimum value of zero for the 12 units, indicating that the transmitted light has an impressive degree of linear polarization. On the other hand, the polarization angle of the transmitted light is maintained at 90°. Thus, LP light with an arbitrary direction of polarization can be easily achieved by changing the orientation of the units. Therefore, these units enable us to generate various combinations of phases spanning the entire 360° range, in addition to polarization directions covering the entire 360° range. Because of the broadband response of the unit cells [see Figs. 1(e) and 1(f)], these properties can be observed at the wavelength range from 820 to 900 nm.

The ability in flexible manipulation of light phase and linear polarization enables the plasmonic metasurfaces to generate

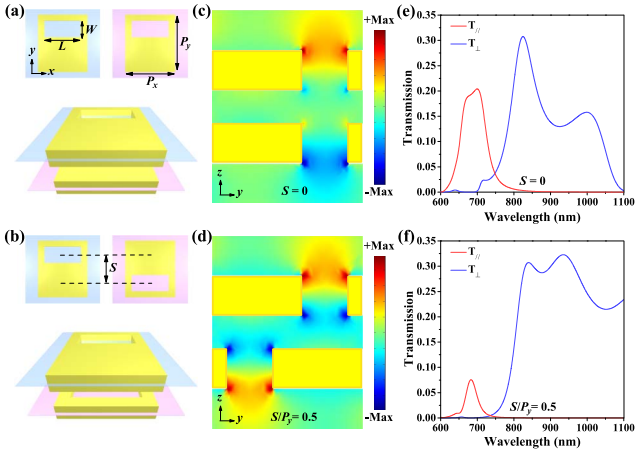

Fig. 1. Schematic of unit cells: top and bottom nanoapertures are (a) aligned and (b) laterally translated by $S = 225$ nm. Blue and pink cross sections correspond to the middle positions for the top and bottom nanoapertures. The period of unit cells in the x and y directions are $P_x = L + 100$ nm and $P_y = 450$ nm. (c), (d) Calculated e-field patterns in the y direction. (e), (f) Calculated transmissions parallel and vertical to the major axis of nanoapertures with $L = 210$ nm and $W = 140$ nm.

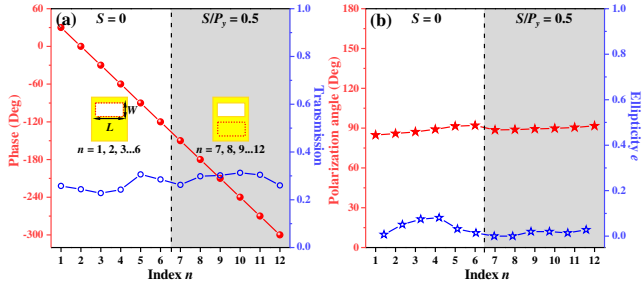

Fig. 2. (a) Transmission phase, amplitude, and (b) polarization states of each unit under CP incident light at a wavelength of 850 nm. The geometric parameters (L, W) of 12 units are (155, 140), (170, 140), (185, 140), (210, 140), (270, 130), (320, 130), (170, 140), (185, 140), (210, 140), (240, 140), (290, 140), and (360, 150) nm. The index n is the number of 12 units. The polarization angle is defined as the angle between the direction of polarization and the x axis.

vector beams through the appropriate selection and space-variant arrangement of the 12 units. In order to demonstrate the effectiveness of the proposed approach, we generated cylindrical vector vortex beams with radial polarization and different topological charge l by arranging different plasmonic metasurfaces excited by normally incident right-handed CP light at a wavelength of 850 nm. As shown in Fig. 3, the plasmonic metasurfaces were divided into six regions corresponding to six types of unit. The spatially varying orientations range from 0° to 360° (clockwise) with a step of 60°, leading to the desired distribution of radial polarization. The process of polarization manipulation introduces the Berry phase, and the phase difference between the units in different regions results in another spatial phase distribution (Φ). Accordingly, the final phase of the generated vector beam is determined by the superposition of the Berry phase and Φ.

The plasmonic metasurface shown in Fig. 3(a) was employed to generate a vector vortex beam with topological charge $l = 1$. The six regions were filled with the same type of unit, which led to $\Phi = 0$. The final spiral phasefront shown in Fig. 3(b) resulting from the Berry phase is characterized by $e^{i\theta}$, where θ is the unit rotation angle. More complicated spiral phase distributions can be formed through adjusting the phase Φ. Figures 3(c) and 3(d) illustrate the case of topological charge $l = 2$. The phase difference between adjacent regions in the clockwise direction is 60°, which equals to θ, leading to $\Phi = e^{i\theta}$. The final helical transmission phase has the form of $e^{2i\theta}$ when considering the Berry phase. Similarly, the radial polarization with topological charge $l = 3$ can also be tailored by utilizing another group of six units, as shown in Figs. 3(e) and 3(f). In this way, we realized the cylindrical vector vortex beams with topological charges $l = 1$, 2, and 3 by designing different spatial phase distributions Φ. Furthermore, by adopting the same method, we are able to realize cylindrical vector vortex beams with other polarization distributions and other topological charges. For instance, the phasefronts with opposite topological charges (i.e., $l = -1, -2, -3$) can be generated by suitably selecting the units with $\Phi = e^{-2i\theta}$, $e^{-3i\theta}$, and $e^{-4i\theta}$.

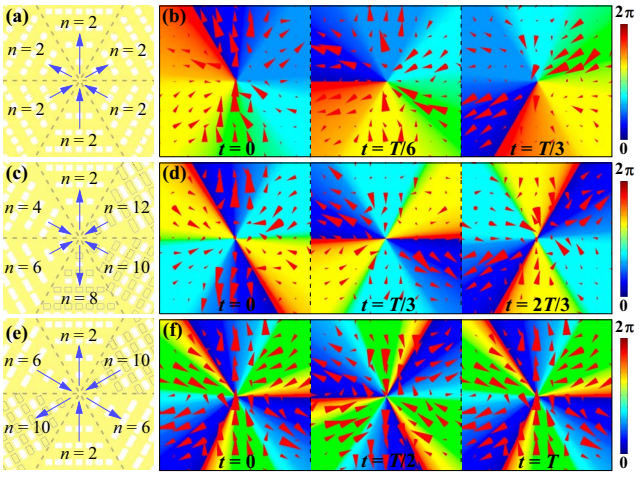

Fig. 3. Schematic models of plasmonic metasurfaces and three calculated instantaneous e-field distributions (red arrows) on the cross section at the distance of 1300 nm from the exit surface with different topological charges: (a), (b) $l = 1$; (c), (d) $l = 2$; (e), (f) $l = 3$. White and yellow rectangles represent the positions of the nanoapertures in two layers. Blue arrows indicate the desired polarization and phase distribution at $t = 0$. Backgrounds of (b), (d), and (f) are the sketch maps of different spiral phase distributions. T is the e-field oscillation period. The transmission phase in the upper region is defined as 0 when its e-field has the largest resonance along the positive direction of the y axis.

When employing the units with conjugate phase $\Phi = e^{-i\theta}$, the locally varying Berry phase can be completely compensated for. This kind of metasurface can generate a vector beam with an identical phase, which corresponds to the situation of topological charge $l = 0$. Figure 4(a) shows the schematic diagram when six regions are filled with six different units, which have a phase difference of –60° between adjacent regions along the clockwise direction. The simulated results of instantaneous transmitted polarization and phase distributions at different moments are given in Fig. 4(b). It can be observed that the transmitted light has a radial polarization distribution. Moreover, the electrical oscillations in the six regions are in phase, resulting from the complete compensation of the Berry phase. Hence, a standard radially polarized vector beam is generated by the designed metasurfaces.

By using the same method, we can also realize the standard azimuthally polarized vector beam by readjusting the six units, as shown in Fig. 4(c). The orientations of the units must start at 90° and increase by a step of 60° (clockwise). The selected six units can also form a spatial phase distribution $\Phi = e^{-i\theta}$ to completely compensate for the Berry phase. Thus, the azimuthal polarization distribution is well generated with an identical phase, as shown in Fig. 4(d).

In addition, the presented plasmonic metasurfaces also exhibit the ability to generate vector optical beams with more complex spatial polarization distributions. We combine 12 units, which were used above, to realize a kind of double-mode vector beam, as an example. The created double-mode vector beam contains a mixture of radially (outer-mode) and azimuthally (inner-mode) polarized vector beams, as indicated in

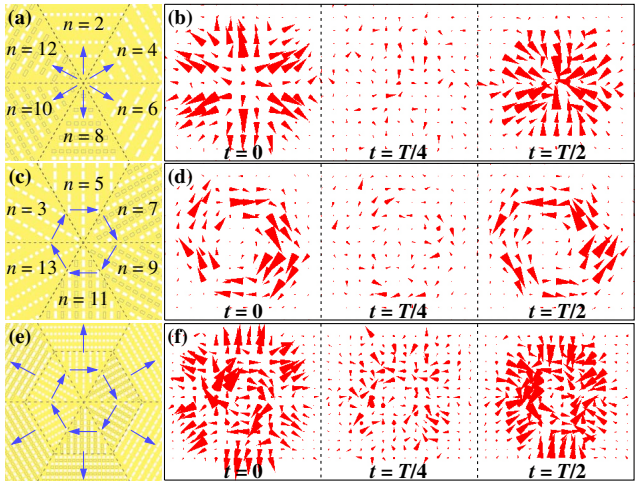

Fig. 4. Schematic models and three calculated instantaneous e-field distributions of (a), (b) radially polarized vector beams; (c), (d) azimuthally polarized vector beams; and (e), (f) a double-mode vector optical beam.

Figs. 4(e) and 4(f). It reveals that the proposed method provides more degrees of freedom to generate arbitrary vector beams. The number of regions and the input circular polarization handedness can be flexibly changed. By increasing the number of divided regions, the resolution of phase and polarization distributions can be further improved. For another case of left-handed CP light illumination, the units should be arranged in a counterclockwise direction to generate the desired vector beams; this is because the sign of the Berry phase depends on the input circular polarization handedness.

In conclusion, we have demonstrated the use of compact plasmonic metasurfaces to generate vector beams with arbitrary spatial variation of phase and linear polarization at the nanoscale. Such a plasmonic metasurface serves a convenient way to simultaneously manipulate the polarization and phase of light. Different varieties of vector beams can be realized through simple alterations in the design of the plasmonic metasurfaces. This novel and flexible method of vector beam generation will have wide applications in optical manipulation, imaging, and super-resolution microscopy, among other fields.

Funding. Chinese National Key Basic Research Special Fund (2011CB922003); International Science & Technology Cooperation Program of China (2013DFA51430); National Basic Research Program (973 Program) of China (2012CB921900); National Science Fund for Talent Training in Basic Sciences (J1103208); National Natural Science Foundation of China (NSFC) (11304163, 61378006); Natural Science Foundation of Tianjin (13JCQNJC01900); Program for New Century Excellent Talents in University (NCET-13-0294); 111 project (B07013).

REFERENCES

1. C. Pfeiffer, N. K. Emani, A. M. Shaltout, A. Boltasseva, V. M. Shalaev, and A. Grbic, Nano Lett. **14**, 2491 (2014).
2. Z. Liu, S. Chen, J. Li, H. Cheng, Z. Li, W. Liu, P. Yu, J. Xia, and J. Tian, Opt. Lett. **39**, 6763 (2014).
3. B. Walther, C. Helgert, C. Rockstuhl, F. Setzpfandt, F. Eilenberger, E.-B. Kley, F. Lederer, A. Tünnermann, and T. Pertsch, Adv. Mater. **24**, 6300 (2012).
4. N. Yu, P. Genevet, M. A. Kats, F. Aieta, J.-P. Tetienne, F. Capasso, and Z. Gaburro, Science **334**, 333 (2011).
5. L. Huang, X. Chen, H. Mühlenbernd, G. Li, B. Bai, Q. Tan, G. Jin, T. Zentgraf, and S. Zhang, Nano Lett. **12**, 5750 (2012).
6. J. Sun, X. Wang, T. Xu, Z. A. Kudyshev, A. N. Cartwright, and N. M. Litchinitser, Nano Lett. **14**, 2726 (2014).
7. Y. Yang, W. Wang, P. Moitra, I. I. Kravchenko, D. P. Briggs, and J. Valentine, Nano Lett. **14**, 1394 (2014).
8. N. Shitrit, S. Nechayev, V. Kleiner, and E. Hasman, Nano Lett. **12**, 1620 (2012).
9. A. Shaltout, J. Liu, V. M. Shalaev, and A. V. Kildishev, Nano Lett. **14**, 4426 (2014).
10. H. Cheng, S. Chen, P. Yu, J. Li, B. Xie, Z. Li, and J. Tian, Appl. Phys. Lett. **103**, 223102 (2013).
11. Y. Zhao and A. Alù, Nano Lett. **13**, 1086 (2013).
12. G. Wu, F. Wang, and Y. Cai, Phys. Rev. A **89**, 043807 (2014).
13. M. G. Donato, S. Vasi, R. Sayed, P. H. Jones, F. Bonaccorso, A. C. Ferrari, P. G. Gucciardi, and O. M. Maragó, Opt. Lett. **37**, 3381 (2012).
14. C. Min, Z. Shen, J. Shen, Y. Zhang, H. Fang, G. Yuan, L. Du, S. Zhu, T. Lei, and X. Yuan, Nat. Commun. **4**, 2891 (2013).
15. H. P. Urbach and S. F. Pereira, Phys. Rev. Lett. **100**, 123904 (2008).
16. P. Yu, S. Chen, J. Li, H. Cheng, Z. Li, and J. Tian, Opt. Express **21**, 20611 (2013).
17. M. Suzuki, K. Yamane, K. Oka, Y. Toda, and R. Morita, Opt. Express **22**, 16903 (2014).
18. C. Varin and M. Piché, Appl. Phys. B **74**, S83 (2002).
19. H. Chen, J. Hao, B. F. Zhang, J. Xu, J. Ding, and H. T. Wang, Opt. Lett. **36**, 3179 (2011).
20. J. Qi, X. Li, W. Wang, X. Wang, W. Sun, and J. Liao, Appl. Opt. **52**, 8369 (2013).
21. S. Chen, X. Zhou, Y. Liu, X. Ling, H. Luo, and S. Wen, Opt. Lett. **39**, 5274 (2014).
22. Z. Bomzon, G. Biener, V. Kleiner, and E. Hasman, Opt. Lett. **27**, 285 (2002).
23. M. Kang, J. Hao, B. Zhang, J. Xu, J. Ding, and H. Wang, J. Opt. Soc. Am. B **29**, 572 (2012).
24. Z. Zhao, J. Wang, S. Li, and A. E. Willner, Opt. Lett. **38**, 932 (2013).
25. G. Li, M. Kang, S. Chen, S. Zhang, E. Y.-B. Pun, K. W. Cheah, and J. Li, Nano Lett. **13**, 4148 (2013).
26. E. Karimi, S. A. Schulz, I. D. Leon, H. Qassim, J. Upham, and R. W. Boyd, Light Sci. Appl. **3**, e167 (2014).
27. C.-F. Chen, C.-T. Ku, Y.-H. Tai, P.-K. Wei, H.-N. Lin, and C.-B. Huang, Nano Lett. **15**, 2746 (2015).
28. M. V. Berry, Proc. R. Soc. London Ser. A **392**, 45 (1984).
29. X. Yi, X. Ling, Z. Zhang, Y. Li, X. Zhou, Y. Liu, S. Chen, H. Luo, and S. Wen, Opt. Express **22**, 17207 (2014).
30. E. D. Palik, *Handbook of Optical Constants of Solids* (Academic, 1998).
31. *COMSOL Multiphysics User's Guide*, Version 3.5 (Comsol AB, 2008).
32. J. Li, S. Chen, H. Yang, J. Li, P. Yu, H. Cheng, C. Gu, H.-T. Chen, and J. Tian, Adv. Funct. Mater. **25**, 704 (2015).